Impact of boiler load and limestone addition on SO_3 and corrosive cold-end deposits in a coal-fired CFB boiler

Vainio, Emil; Vänskä, Kyösti; Laurén, Tor; Yrjas, Patrik; Coda Zabetta, Edgardo; Hupa, Mikko; Hupa, Leena

Published in:
Fuel

DOI:
10.1016/j.fuel.2021.121313

Published: 15/11/2021

Document Version
Final published version

Fuel 304 (2021) 121313

Contents lists available at ScienceDirect

Fuel

journal homepage: www.elsevier.com/locate/fuel

Full Length Article

Impact of boiler load and limestone addition on SO_3 and corrosive cold-end deposits in a coal-fired CFB boiler

Emil Vainio [a,*], Kyösti Vänskä [b], Tor Laurén [a], Patrik Yrjas [a], Edgardo Coda Zabetta [b], Mikko Hupa [a], Leena Hupa [a]

[a] Johan Gadolin Process Chemistry Centre, Laboratory of Molecular Science and Engineering, Åbo Akademi University, Biskopsgatan 8, FI-20500 Åbo-Turku, Finland
[b] Sumitomo SHI FW Energia Oy, Varkaus 78201, Finland

ARTICLE INFO

Keywords:
Cold-end corrosion
SO_3
H_2SO_4
Hygroscopic deposits
NH_4Cl
$CaCl_2$

ABSTRACT

The risk of cold-end corrosion caused by two different phenomena was studied: the well-known sulfuric acid-induced corrosion and corrosion caused by hygroscopic fly ash deposits. Measurements were performed in a full-scale circulating fluidized bed boiler firing bituminous coal with high contents of sulfur and chlorine. The boiler was run both with and without limestone addition to reveal the effects of limestone on corrosion. Furthermore, the impact of boiler load on corrosion and deposit composition was studied. Corrosion probe, SO_3, and dew point measurements were performed up- and downstream of the electrostatic precipitator. Ash deposits were collected from the different sides of the corrosion probe and were analyzed. The formation of SO_3 was low in all cases (<0.1 ppm_v), which was connected to the relatively low furnace temperature in fluidized bed combustion and the efficient SO_3 capturing of the fly ash and limestone. The different operational parameters of the boiler had a significant impact on deposit composition and on expected corrosion risk. At full load and without limestone addition, the chlorine of the fuel stayed as gaseous HCl, whereas no Cl was found in the deposits. However, when limestone was added, corrosion was caused by the presence of deliquescent calcium chloride. At low load operation of the boiler, ammonium chloride was formed on the cold-end deposit probe. Ammonium chloride was formed via the reaction between HCl and NH_3 in the cooling flue gases. Laboratory studies with NH_4Cl was further conducted to assess its corrosivity.

1. Introduction

Cold-end corrosion in combustion can generally be caused by an acid condensing on steel surfaces or hygroscopic deposits that absorb moisture from the flue gases. This may occur if the material temperature is kept too low. On the other hand, efficient use of energy in flue gases is of importance in order to recover as much energy as possible. An effective way is to lower the boiler exit flue gas temperature, since every 10 °C drop in the flue gas temperature could potentially increase the boiler thermal efficiency by about 0.5%. However, lowering the temperature of the flue gases can lead to corrosion - referred to as low-temperature corrosion or cold-end corrosion - of pre-heaters, flue gas cleaning equipment, and other parts of the flue gas channel. One of the main concerns with respect to lowering the flue gas temperature in coal-fired power plants is the sulfuric acid dew point. If the temperature of metal surfaces is lower than the sulfuric acid dew point, severe corrosion might occur [1,2]. Several factors influence the formation of SO_3. In coal and biomass combustion, the ash plays an important role in the flue gas SO_3 concentration [3,4]. Sulfur trioxide can be captured by the alkaline oxides in the ash to form sulfates [5–9]. On the other hand, the ash forming matter may also contribute to the catalytic conversion of SO_2 to SO_3 [6,10]. The extent of SO_3 formation depends also on the furnace temperature and residence time [11], the SO_2 concentration in the flue gas, the excess oxygen [11,12], certain additives, and the use of selective catalytic reduction (SCR) of NO_X emissions [13]. In fluidized bed combustion, the furnace temperature is relatively low, leading to low homogeneous conversion of SO_2 to SO_3 [4]. Another issue related to selective catalytic reduction (SCR) of NO_X emission is the formation of ammonium bisulfate from SO_3 and NH_3 slip. Ammonium bisulfate is sticky and may lead to plugging and corrosion in the cold-end [14,15].

When the flue gas temperature drops below some 500 °C, any SO_3 formed will start reacting with water vapor forming gaseous H_2SO_4 and at about 200 °C all SO_3 will be converted to H_2SO_4(g) [16]. The sulfuric acid dew point depends on the concentrations of H_2SO_4(g) and H_2O. For

* Corresponding author.
E-mail address: emil.vainio@abo.fi (E. Vainio).

https://doi.org/10.1016/j.fuel.2021.121313
Received 25 February 2021; Received in revised form 20 May 2021; Accepted 19 June 2021
Available online 17 August 2021

example, in a flue gas with 10 vol% H_2O and H_2SO_4(g) varying between 1 and 5 ppm_v, the acid dew point would be 116–131 °C (calculated with correlation by Verhoff and Banchero [17]). In this paper, both gaseous H_2SO_4 and SO_3 are referred to as SO_3.

Cold-end corrosion can also be caused by hygroscopic deposits. Especially in biomass combustion, hygroscopic deposits have been shown to cause corrosion in the cold-end [4,18–22]. Recently it was shown by Pan et al. [23], that corrosion of heat transfer tubes in the cold-end of a coal-fired boiler was caused by chlorides in the deposit. The corrosion could not be explained by HCl condensing on the surfaces since the conditions were well above the dew point of HCl [23]. Hygroscopic and deliquescent salts can absorb water from the flue gas. Subsequently, this process may lead to wet corrosion. Deliquescent salts absorb, at a certain relative humidity, enough water to fully dissolve in the water. The relative humidity at which the salt transforms from a solid to a salt solution is called the deliquescent relative humidity (DRH). Deliquescent salts that have been reported to cause cold-end corrosion are, e.g., $CaCl_2$ [4,18], $ZnCl_2$ [18], K_2CO_3 [22], and $NaHSO_4$ [20]. Hygroscopic and deliquescent deposits may also cause deposit build-up in the cold-end of boilers [24].

There is an increased need to operate boilers at varying loads to cope with the power demand and to use additives to mitigate emissions. All this may have an impact on ash deposits and heat exchanger material corrosion in the cold-end of the boiler. The changes in the combustion process may lead to the formation of hygroscopic and corrosive deposits in the cold-end and may also affect the SO_3 formation. In this work, two different kinds of cold-end corrosion phenomena were studied. On one hand the well-known sulfuric acid-induced low-temperature corrosion. One the other hand the more recently identified corrosion caused by hygroscopic fly ash deposits. Measurements were performed in a full-scale circulating fluidized bed (CFB) boiler burning bituminous coal. The tests were conducted at full and partial boiler load, and with and without limestone feeding. Dew-point measurements and measurements of SO_3/H_2SO_4(g) were conducted before and after the electrostatic precipitator (ESP). Additionally, short-term corrosion probe measurements were performed to determine the corrosion rate of carbon steel at different material temperatures. Deposits from the probe were collected and analyzed to determine the effect of boiler operation on deposit composition. Under some conditions, a major part of the deposit surprisingly consisted of ammonium chloride. This compound is here first time found under conditions with no ammonia addition applied, and the mechanisms of how this can be formed and cause corrosion is also discussed.

2. Experimental

2.1. Boiler and fuel

The measurements were conducted in a full-scale CFB power boiler burning bituminous coal. Measurements of SO_3/H_2SO_4(g), dew point, and corrosion probe measurements were performed before and after the ESP, Fig. 1. The boiler was operated in three modes (Table 1): 1) full load without limestone addition, 2) 55% load without limestone addition, 3) full load with limestone addition. No ammonia/ammonium based additives, SCR, SNCR, or other additives than limestone were used in the boiler. The fuel properties are presented in Table 2. The ash content of the fuel was high, 16.5 wt%. The sulfur and chlorine contents of the fuel were 1.57 wt% and 0.64 wt%, respectively. X-ray fluorescence (XRF) analysis results of the ashed fuel are shown in Table 3. The fuel ash has a relatively high iron oxide content, 9.4 wt%. Iron oxide may catalyze the SO_2 to SO_3 conversion in the furnace [6]. Vanadium is also known to catalyze the formation of SO_3 [25]; however, the concentration of

Table 1
Experimental cases during the measurement campaign.

Case	Limestone feed	Load
1	Limestone off	Full
2	Limestone off	Low (~55%)
3	Limestone on	Full

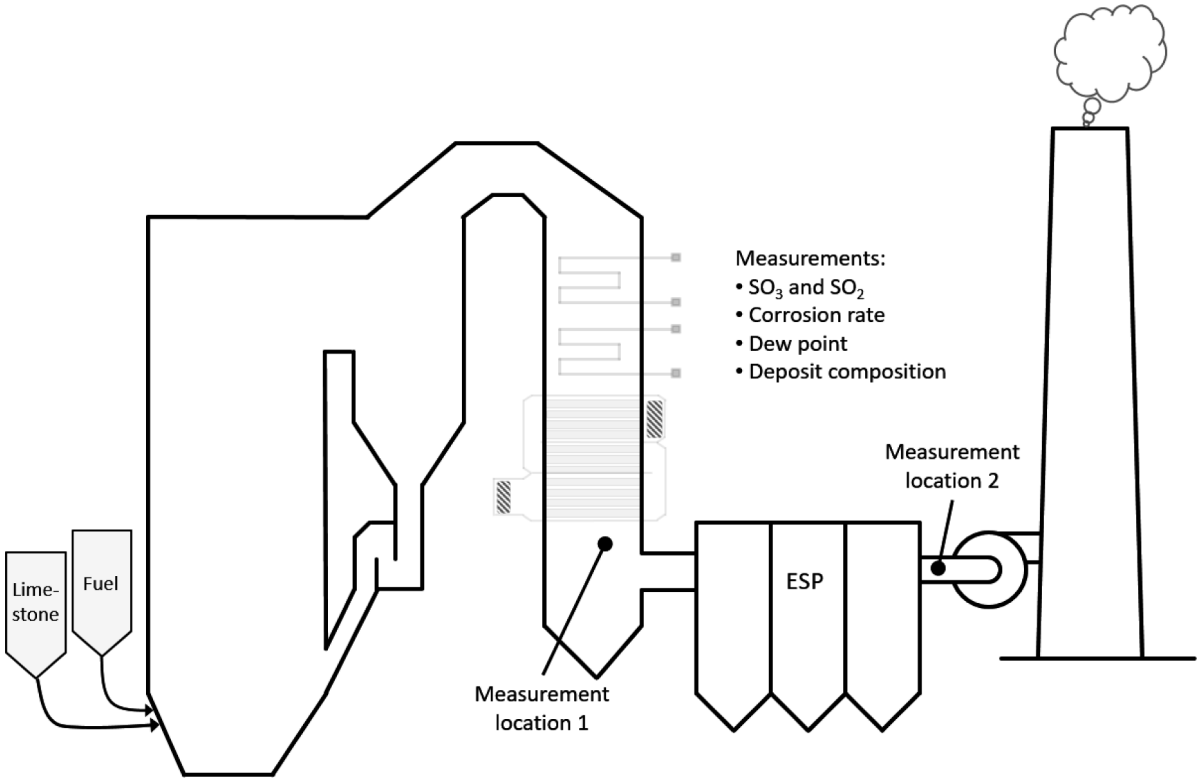

Fig. 1. Measurement locations and measurements in the CFB boiler.

Table 2
Fuel properties. All numbers, except moisture, are expressed on a dry basis.

Total moisture	wt%	24.8
Ash content (815 °C)	wt%	16.5
Volatile matter	wt%	31.7
Gross calorific value	MJ/kg	26.27
C	wt%	64.8
H	wt%	4.2
N	wt%	1.02
S	wt%	1.57
O (calculated)	wt%	11.3
Cl	wt%	0.64

Table 3
XRF analyses of laboratory ash produced at 550 °C, presented as oxides. Numbers in wt% on a dry basis.

Compound	Wt% db
Al_2O_3	23.3
CaO	3.86
FeO	9.37
K_2O	2.17
MgO	1.99
MnO	0.031
Na_2O	3.38
P_2O_5	0.16
SO_3	9.89
SiO_2	48.0
TiO_2	1.15
V_2O_3	0.041
ZrO_2	0.047

vanadium was low in the fuel. Calcium in the fuel has a dominant role in sulfur capture in coal combustion [26]. The molar ratio of Ca/S in the fuel was 0.55. Sulfur can also be captured by Mg, K, and Na in the fuel. The (Ca + Mg + 2Na + 2 K)/S molar ratio was 1.6. However, a large part of the sodium and potassium in the fuel is present as alkali aluminosilicates in coal or is captured by aluminosilicates in the combustion and is thus not available for sulfur capture [27,28].

2.2. Measurement techniques

2.2.1. SO_3 measurements

A recently developed salt method was used to detect SO_3 and H_2SO_4(g) [4,29]. In this method, a cartridge filled with KCl powder is placed in the tip of a probe. The probe is inserted in the flue gas stream and the flue gases are pulled through the salt layer. Under the experimental conditions, the KCl will selectively react with any SO_3 or sulfuric acid in the gas to form K_2SO_4 and/or $KHSO_4$. No reaction with SO_2 will take place. As the amount of potassium sulfate corresponds to the SO_3 or H_2SO_4(g) in the gas sample, the total SO_3 can be calculated when the total amount of gas pulled through the salt is known. The sampling time varied between 15 and 70 min, and the flow of gas pulled through the salt was about 1 Nl/min. The detection limit depends on the amount of flue gas volume sampled. In this work the detection limit was about 1–3 ppb_v SO_3. The method is described in detail in Vainio et al. [4]. The probe is kept slightly tilted to avoid water condensate from the cold-end of the probe to flow to the KCl tube (Fig. 2). Water in the salt would lead to a measurement error by SO_2 absorption in the water and subsequently oxidization to sulfate. After the measurement, the salt cartridges were transported to the laboratory and dissolved in 20 ml of deionized distilled water. The sulfate concentration was determined by ion chromatography with conductivity detection (Metrosep anion Dual 2 column and a 732 IC detector by Metrohm). Six analyzes were made for every sample to prove the repeatability. Sulfur dioxide was measured by absorbing it in two impinger bottles with 5 vol% hydrogen peroxide (H_2O_2). The sulfate formed in the solution was analyzed in the same manner as the KCl trap.

2.2.2. Dew point measurements

The dew point temperature in the flue gases was measured by the Lancom 200 dew point meter. The probe has a sensor in the tip, which gives a signal when condensate forms on it. The probe tip is inserted into the flue gas channel, and the temperature is slowly decreased until the dew point is reached. The detection limit of the device is typically 5 ppm_v of SO_3 or a dew point of 125 °C – depends on the application – and uncertainty ± 0.5 °C.

2.2.3. Corrosion/deposit probe

An air-cooled short-term corrosion probe was used to quantify the initial corrosion rate of carbon steel (P235GH) at various material temperatures (50–100 °C). The maximum temperature fluctuation in the sample was ± 2 °C. The method is described in detail in Vainio et al. [4]. The exposure time was 2 h. Windward, side, and leeward deposits were collected and analyzed by means of scanning electron microscopy with energy-dispersive X-ray spectroscopy (SEM-EDX), LEO Gemini 1530

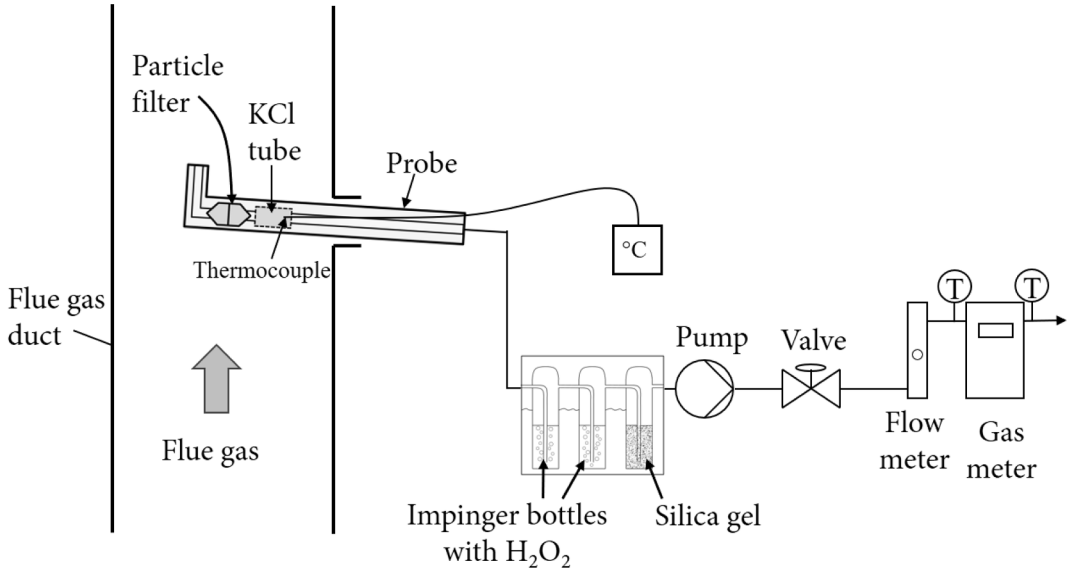

Fig. 2. In-situ measurement setup of the salt method for the measurement of SO_3 and H_2SO_4(g). Modified from [4].

with a Thermo Scientific UltraDry Silicon Drift Detector (SDD). To quantify the material loss, the corrosion products were removed first with deionized distilled water followed by drying with acetone. The remaining corrosion products were removed with citric acid in an ultrasonic bath for 10 min. The acid step was repeated until all corrosion products were removed. Blank samples were used to quantify any metal loss of the sample. A description of the method can be found in Laurén [30]. After the acid wash, the samples were rinsed with deionized distilled water and dried with acetone. After the washing procedure, the total weight loss of the corrosion rings were used to calculate an average corrosion rate for the exposed surface.

2.2.4. Corrosion tests in the laboratory

Corrosion tests were done to study the corrosivity of hygroscopic NH_4Cl. Carbon steel coupons (P235GH) with the dimensions 20 mm × 20 mm × 5 mm were used. The coupons were first polished in ethanol with a 320 grit silicon carbide paper and then with a 1000 grit paper, and finally with a 2500 grit paper. The coupons were washed in an ultrasonic bath in ethanol. Three coupons per test were used and 100 mg of salt was placed on top of the coupons. The experiments were conducted with 10 vol% water vapor, 5 vol% O_2 and rest N_2 in the temperature range of 60 to 80 °C. A stable flow of water vapor was produced with a Cellkraft P-2 humidifier. The coupons were first heated in a nitrogen atmosphere to the desired temperature. When the temperature was stable, water vapor and oxygen were added to the gas. The total flow was 2 l/min (NTP) and the exposure time was 4 h. After the exposure, the salt was washed off with deionized distilled water and the steel coupons were dried with acetone. The surface and corrosion products were analyzed using an SEM-EDX. The corrosion products were removed in the same manner as for the corrosion rings in section 2.2.3 and the weight loss was measured. From the weight loss an average corrosion rate was calculated for the exposed area.

3. Results

3.1. SO_3 and dew point measurements

During the first experimental case at full load, the limestone feed was off; thus, the SO_2 was relatively high, on average 810 ppm_v. Despite the high SO_2, the concentrations of SO_3 both before and after the ESP were below 0.1 ppm_v (Fig. 3). The SO_3 concentration was on an average 0.057 ppm_v upstream of the ESP and 0.033 ppm_v downstream of the ESP. The reason for these low SO_3 concentrations was partly caused by the relatively low temperature in the furnace leading to a low homogeneous conversion of SO_2 to SO_3. The average furnace temperature was 815 °C and the residence time in the furnace was 5.6 s for Case 1. A low homogeneous SO_2 to SO_3 conversion was shown by Fleig et al. [11] in laboratory experiments made at similar temperature and residence time. In their study, the homogeneous conversion of SO_2 to SO_3 in a flow reactor was 0.3% at 827 °C, 1000 ppm_v SO_2, 3 vol% O_2, 8.7 vol% H_2O, and a residence time of 5 s [11]. Furthermore, the very low SO_3 concentrations in our work can also be explained by the ability of the alkali and alkaline earth metals, which are not present as silicates, to capture the SO_3 that is formed. The (Ca + Mg + 2Na + 2 K)/S molar ratio was 1.6.

No sulfuric acid dew point could be detected with the dew point meter for case 1. However, a signal was obtained between 50 and 62 °C. The water vapor concentration in the flue gas was on average 10 vol% corresponding to a pure water dew point of 46 °C. The elevated measured dew point could be caused by fluctuations in the water vapor in the flue gas or hygroscopic deposit formation on the sensor leading to a wet deposit and consequently a signal. It is unlikely that the signal was caused by HCl condensation. The HCl dew point is just above the water dew point, e.g. in a gas with 10 vol% H_2O and 100 to 500 ppm_v HCl, the HCl dew point would be between 49 and 53 °C [31]. Unfortunately, the plant FTIR was unavailable during the measurement campaign, and thus the HCl concentration in the flue gas is not available. Based on previous experience of the CFB boiler, the HCl level in the measurement location at same conditions as in the measurement campaign is about 300 ± 25 ppm_v. The calculated sulfuric acid dew point from the average SO_3 concentration measured after the ESP (0.033 ppm_v) and 10 vol% H_2O is 87 °C (calculated with the correlation by Verhoff and Banchero [17]). It has to be noted that the correlation has not been validated for this low concentrations. Therefore, the dew point should be interpreted with caution. It is also unlikely that enough condensate would form on the sensor to create a signal.

At low load and without limestone addition (Case 2), the SO_3 concentrations were on average 0.007 ppm_v upstream of the ESP and 0.001 ppm_v downstream of the ESP (Fig. 4). The average furnace temperature was much lower, 740 °C, compared to the full load cases. This could explain the lower SO_3 in the flue gas. A signal with the dew point meter was obtained between 48 and 52 °C, thus no sulfuric acid dew point was

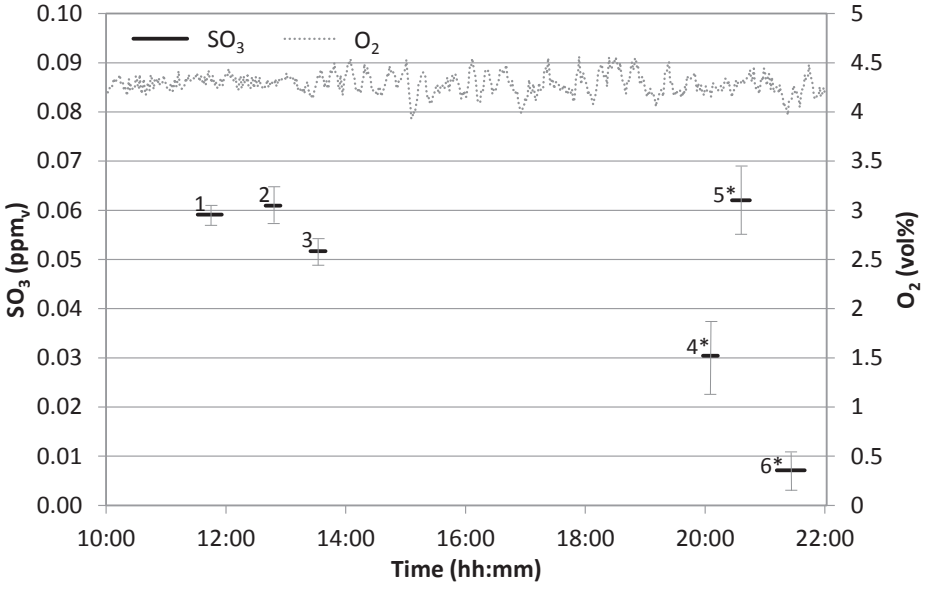

Fig. 3. SO_3 measured before and after (indicated by *) the ESP and O_2 measured in the stack during Case 1 (limestone off and full load). The average SO_2 in the flue gas was 810 ppm_v.

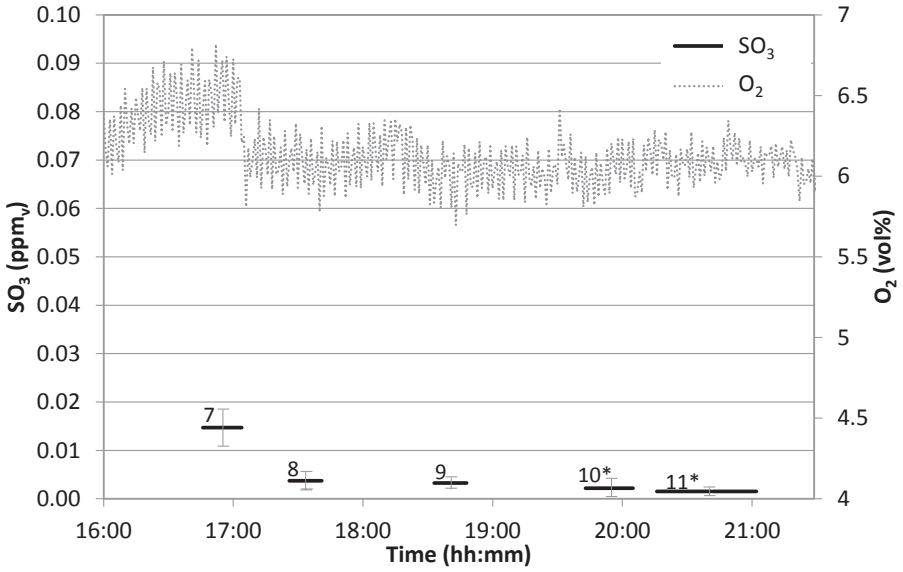

Fig. 4. SO_3 measured before and after (indicated by *) the ESP and O_2 measured in the stack during Case 2 (limestone off and low load). The average SO_2 in the flue gas was 810 ppm_v.

detected. When limestone was used during full load (Case 3), SO_2 was on average 60 ppm_v, and SO_3 was on average 0.013 ppm_v upstream of the ESP and 0.009 ppm_v downstream of the ESP (Fig. 5). The average furnace temperature was 820 °C. A signal with the dew point meter was obtained at 55 °C, and no sulfuric acid dew point was detected. In all cases, a signal was observed just above the water dew point and this could be attributed to hygroscopic dust formation on the sensor and the subsequent absorption of water. The HCl dew point could partly explain the dew point reading; however, this could not be confirmed.

Fig. 6 summarizes the SO_3 measurements for the different boiler operations. Even if the SO_3 concentrations are for practical purposes insignificantly low, interestingly some differences could be seen depending on the conditions. The lower SO_3 concentrations downstream of the ESP in the different cases are probably caused by the capture of some SO_3 by the ash in the ESP. The load and limestone also had an impact on the SO_3 concentration. At low load the furnace temperature was 80–90 °C lower than during full load operation, resulting in a lower homogeneous SO_2 to SO_3 conversion. A dramatic change in the cold-end ash composition was also observed during low load operation; the deposits were rich in ammonium chloride (see section 3.2.2). The presence of NH_3 in the flue gas can also strip the SO_3 by forming ammonium sulfates. Comparing the cases with full load in Fig. 6, the SO_3 concentrations were lower with limestone addition, due to the capture of SO_2 and SO_3 by the additive.

3.2. Corrosion probe measurements and hygroscopic fly ash deposits

The initial corrosion rates in μm/h are summarized in Fig. 7. 0.1 μm/h corresponds to 0.88 mm wall thickness loss per year when extrapolated linearly (8760 h). Usually, the initial corrosion rate is higher than

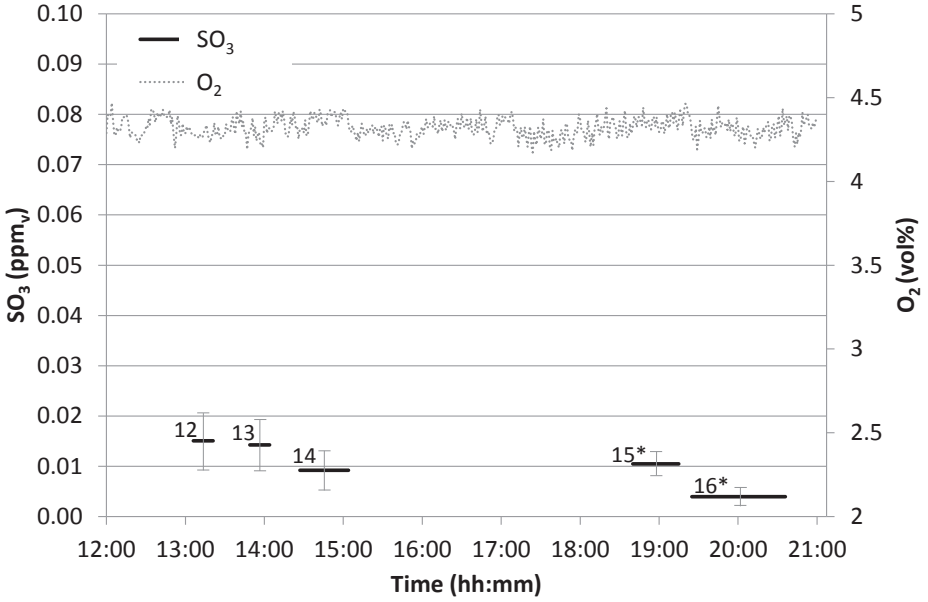

Fig. 5. SO_3 measured before and after the ESP (indicated by *), and SO_2 and O_2 were measured in the stack during Case 3 (limestone on and full load). The average SO_2 in the flue gas was about 60 ppm_v (dry gas).

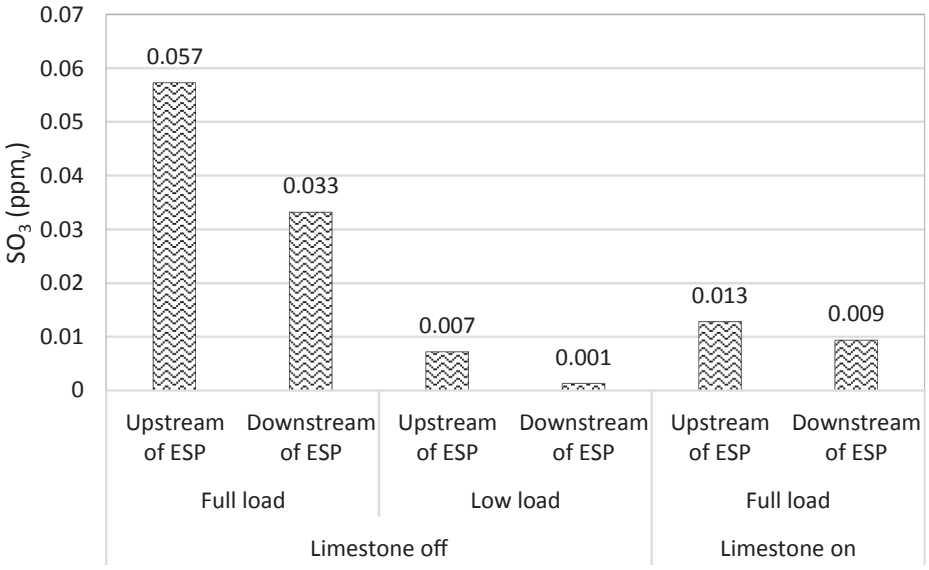

Fig. 6. Summary of the average SO_3 concentration measured upstream and downstream of the ESP for the different cases.

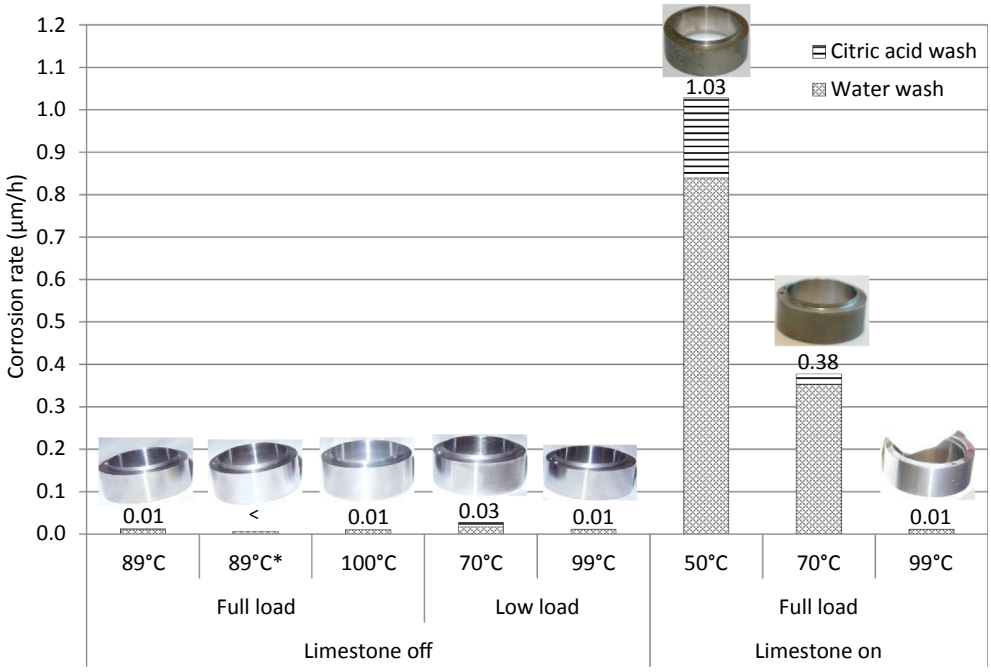

Fig. 7. Summary of initial corrosion rates in µm/h and pictures of the side of the washed corrosion rings. The measurement marked with * is measured downstream of the ESP.

the rate measured after a longer exposure. Nevertheless, the rates suggest that the corrosion is mild with material temperatures between 70 and 100 °C when operating without limestone addition. The corrosion is more severe with limestone addition, thus clearly indicating that the corrosion risk is not associated with sulfuric acid condensation. Instead, this corrosion is connected to the formation of hygroscopic deposits when limestone is used.

3.2.1. *Full load operation (Case 1)*

At full load and no limestone addition, no clear corrosion was observed in the temperature range of 89–100 °C. The two measurements, which were done before the ESP with material temperatures of 89 and 100 °C, indicated very mild corrosion, ~0.01 µm/h. While removing the probe from the flue gas channel, most of the deposit was removed from the probe due to the draft in the measurement opening. Thus, the rings had a thin layer of deposit on the windward side and the side of the ring. Due to the minor deposit amounts, samples could be collected only from the leeward side of the rings. The EDX analyses of the leeward deposits are presented in Fig. 8. The deposits consisted mainly of aluminosilicates, while no chlorine was present. This is caused by the sulfation of alkali chlorides releasing HCl [32]. Corrosion was not observed in the probe measurement after the ESP at 89 °C and no deposit samples could be collected due to the low deposit build-up. The average SO_3 measured before the ESP was 0.056 ppm_v and the water vapor concentration was 10 vol%. This would result in a theoretical acid dew point of 92 °C, as estimated with the correlation by Verhoff and Banchero [17]. However, the correlation is not verified for this low SO_3 concentrations. Also, the amount of condensing acid would be extremely

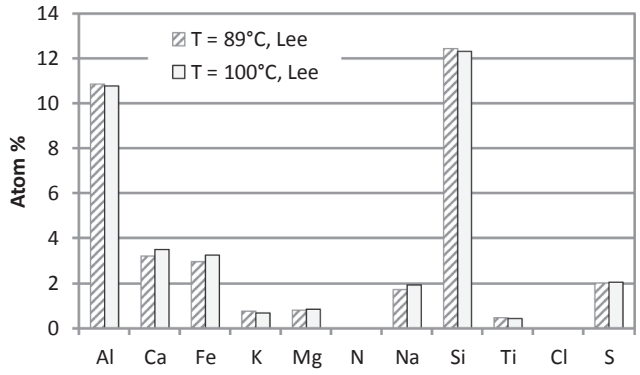

Fig. 8. EDX analyses of the leeward deposits collected upstream of the ESP (measurement location 1) with material temperatures of 89 and 100 °C during Case 1 (limestone off and full load).

small, thus it is unlikely that this low SO_3 would cause any corrosion in the presence of a deposit. No signs of acid condensation was observed with the material temperature of 89 °C. Longer exposure times would be needed to confirm this.

3.2.2. *Ammonium chloride formation (Case 2)*

Two corrosion probe measurements were conducted during low load conditions and without limestone addition (Case 2). The measurements were done before the ESP and the material temperatures were adjusted to 70 °C and 99 °C. The corrosion was mild in both tests, however, with a material temperature of 70 °C, a clear discoloration of the ring was observed on the side and leeward side. The corrosion was still mild based on the weight loss and the corrosion rate was 0.03 μm/h. It seems that the discoloration appeared in the same location as only some deposit had gathered on the ring. Interestingly, the deposits were rich in chlorine, mainly in the form of NH_4Cl. As can be seen in Fig. 9, the main deposit components were nitrogen and chlorine and in almost the same atomic ratio. Ammonium chloride in the deposit is formed from NH_3(g) and HCl(g) present in the gas (reaction (1)). The reaction pathway for NH_4Cl(s) formation in the cold-end of this study is illustrated in Fig. 10a. There was no NH_3 injection in the boiler during the measurements. However, NH_3 is a known intermediate nitrogen species in the reactions of fuel nitrogen to NO_X and N_2 [33]. A part of the NH_3 released from the coal particles during the combustion remained unreacted throughout the boiler due to the lower temperatures in the boiler as a consequence of the low load; the average furnace temperature was 740 °C, which was 80–90 °C lower compared to the full load cases.

$$NH_3(g) + HCl(g) \leftrightarrow NH_4Cl(s) \quad (1)$$

The stability of NH_4Cl as a function of temperature at various NH_3 and HCl concentrations is shown in Fig. 11. Ammonium chloride is stable even at relatively low concentrations of HCl and NH_3 in the temperature range of the corrosion probe tests. According to thermodynamic calculations, NH_4Cl is stable at 70 °C when the concentrations of both NH_3 and HCl are above about 1 ppm_v. HCl(g) in the measurement location was approximately 300 ppm_v and even at 99 °C, 1 ppm_v NH_3 is enough for NH_4Cl(s) formation. Ammonium chloride has previously been reported to cause low-temperature corrosion in waste incineration using selective catalytic reduction of NO_X [19]. The darker color found on the leeward side of the corrosion ring at 70 °C could originate from hygroscopic NH_4Cl reacting with the steel. The corrosivity of NH_4Cl was further studied in section 3.3.

3.2.3. *Effects of limestone addition (Case 3)*

At full load and limestone addition, the corrosion was more severe. In the measurement upstream of the ESP and with a material temperature of 70 °C the corrosion rate was 0.38 μm/h (corresponding to 3.3 mm/year when extrapolated linearly). The deposit analyses showed high chlorine contents; however, no nitrogen was detected. The deposit compositions were high in both calcium and chlorine (Fig. 12), and the chlorine originated most likely from $CaCl_2$, which is a highly hygroscopic salt. Calcium chloride could form from unreacted calcium oxide and HCl in the gas (reaction (2)). This reaction pathway is illustrated in Fig. 10b. With a material temperature of 70 °C and a water vapor concentration of 10 vol%, $CaCl_2$ deliquesces, i.e. absorbs enough water from the flue gases to fully dissolve in the absorbed water. The conditions at which deliquescence occurs in flue gases are presented in Fig. 13. The corrosion rates from the probe measurements at the various material temperatures are also depicted in the figure. Calcium chloride on carbon steel is highly corrosive at conditions below the deliquescence curve in Fig. 13, and at 10 vol% H_2O deliquescence occurs at 84 °C [35]. Calcium chloride has also been found to cause low-temperature corrosion in biomass boilers [4,18] and at higher water vapor concentrations in the flue gas it may be corrosive well above 100 °C [4,35]. With a material temperature of 50 °C, severe wet corrosion occurred with a corrosion rate of 1.03 μm/h (corresponding to 9.0 mm/year when extrapolated

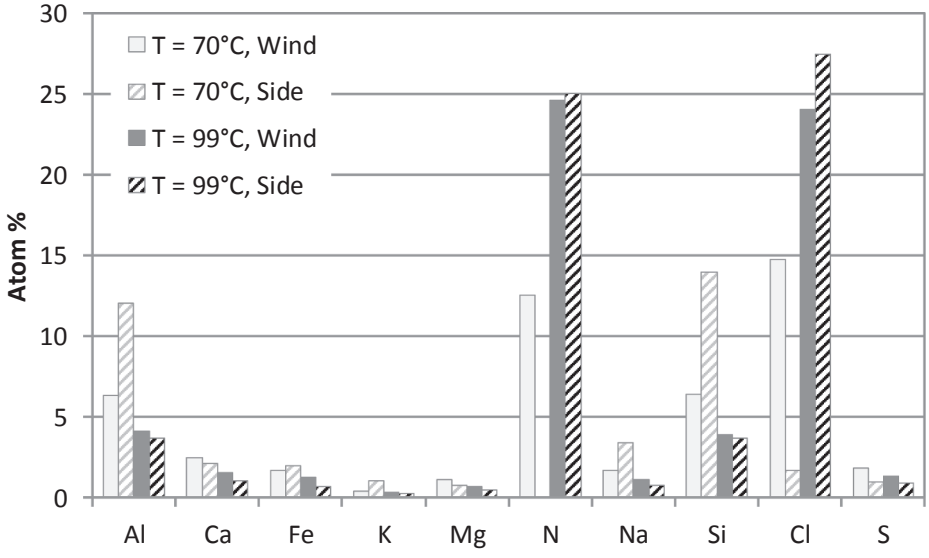

Fig. 9. EDX analyses of side and leeward deposits collected upstream of the ESP (measurement location 1) with material temperatures of 70 and 99 °C during Case 2 (limestone off and low load).

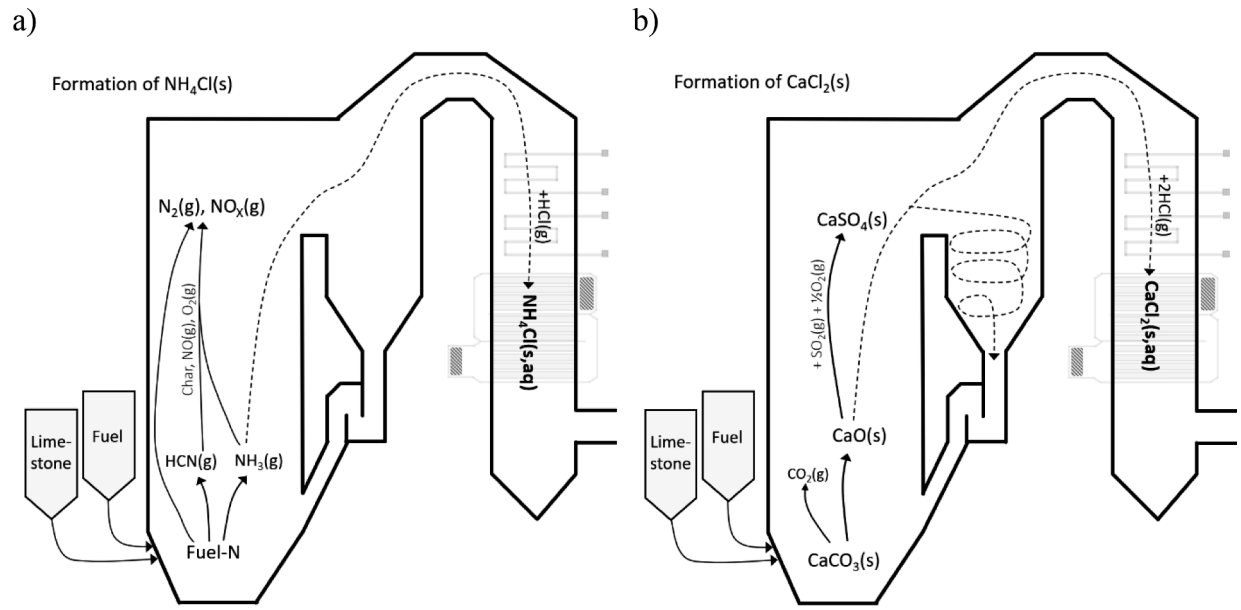

Fig. 10. Reaction pathways for: a) NH_4Cl from fuel nitrogen and chlorine during low load operation and b) $CaCl_2$ from limestone and fuel chlorine in the CFB boiler.

linearly). At 50 °C more water will be absorbed by $CaCl_2$ compared to 70 °C [35], which could also be clearly seen while removing the corrosion probe. Both the lower temperature and higher water absorption will increase the oxygen solubility into the formed solution [36], and consequently the corrosion rate [37]. Furthermore, the increased corrosion rate at 50 °C could be caused by condensation of HCl since the temperature is just below the approximated HCl dew point of 52 °C at 300 ppm_v HCl (Fig. 13). With a material temperature of 99 °C, which is clearly above the deliquescence temperature for $CaCl_2$, no visible corrosion was seen on the corrosion probe ring.

$$CaO(s) + 2HCl(g) \leftrightarrow CaCl_2(s) + H_2O(g) \quad (2)$$

3.3. Corrosion tests in the laboratory

Fig. 14 presents SEM images and photographs of the coupons after exposure to NH_4Cl at 60 °C and 80 °C. In the corrosion experiments with a material temperature of 60 °C and 10 vol% H_2O the steel coupon was heavily corroded. Deliquescence of NH_4Cl did not occur as can be seen from the salt on top of the sample after the exposure. It seems that NH_4Cl is hygroscopic and absorbs only some water at 60 °C and 10 vol% H_2O. Ammonium chloride has been reported to be deliquescent (DRH 76% at 25 °C [38]), however data at flue gas conditions is not available to the authors' knowledge. The absorbed water leads to corrosive conditions since an acidic electrolyte with high conductivity is formed. At 60 °C and 10 vol% H_2O, there was a clear weight gain of 1.66 mg caused by the formation of iron oxide/hydroxide, as seen in the SEM image (Fig. 14a). In Fig. 15, weight changes of P235GH after exposure to NH_4Cl and washing with water followed by removing the corrosion products with citric acid are shown. At 60 °C and after removing the corrosion products with citric acid the weight loss was 5.3 mg corresponding to an average corrosion rate of about 1.2 μm/h, when calculated for the area below the salt. However, corrosion did not only occur below the salt but on the edges of the steel coupon. Thus, the corrosion rate is somewhat overestimated. In the experiments at 70 and 80 °C, corrosion was observed mainly around the salt, as can be seen from the photograph in Fig. 14b. The SEM image in Fig. 14b shows the corroded area around the salt pill after exposure at 80 °C. The SEM image indicates pitting corrosion of the steel. One explanation for the pits around the salt pill could be that NH_4Cl is not stable at the experimental conditions and dissociates to HCl(g) and NH_3(g) [39] because these gases were not present in the inlet gas. This caused locally high HCl(g) and NH_3(g) concentrations around the salt pill and apparently lead to corrosion of the steel. Deposits rich in NH_4Cl in a boiler might cause corrosion by this mechanism if NH_4Cl(s) dissociates due to variations in NH_3(g) and HCl (g) in the flue gas. The corrosion mechanism of NH_4Cl on carbon steel should be studied further.

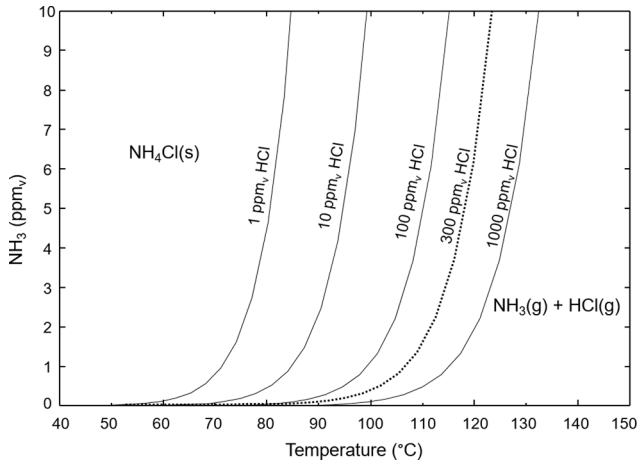

Fig. 11. Stability of NH_4Cl(s) at 1, 10, 100, 300, 1000 ppm_v HCl(g) and 0–10 ppm_v NH_3(g). The calculations were done with the thermodynamics software package FactSage 7.2 [34], using the FToxid database.

The high corrosion rate seen in the full-scale measurements with limestone addition in the boiler (Case 3) and at a material temperature of 70 °C was caused by the deliquescence of $CaCl_2$, which occurs at 84 °C at 10 vol% H_2O [35]. With a probe temperature of 99 °C, i.e. well above the deliquescence temperature of $CaCl_2$ at 10 vol% H_2O, no clear corrosion was observed. In laboratory corrosion experiments with $CaCl_2$ by Vainio et al. [35], corrosion of carbon steel was only seen below the deliquescence temperature. A key difference in the corrosion between NH_4Cl and $CaCl_2$ at conditions when the salt absorbs moisture exist; with NH_4Cl the corrosion product was attached to the exposed area, leading to a weight gain of the sample, while for $CaCl_2$ no corrosion layer was attached to the steel surface. Instead, the corrosion product was mainly

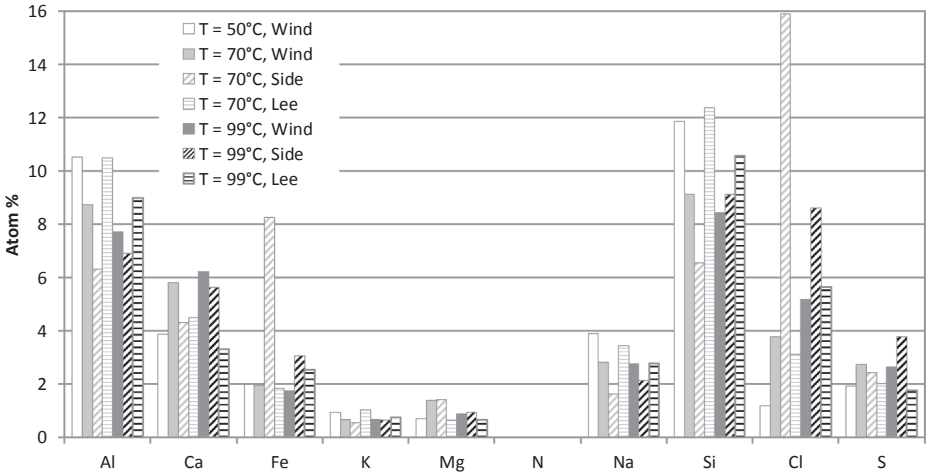

Fig. 12. EDX analyses of deposits collected upstream of the ESP (measurement location 1) with material temperatures of 50, 70, and 99 °C during Case 3 (limestone on and full load).

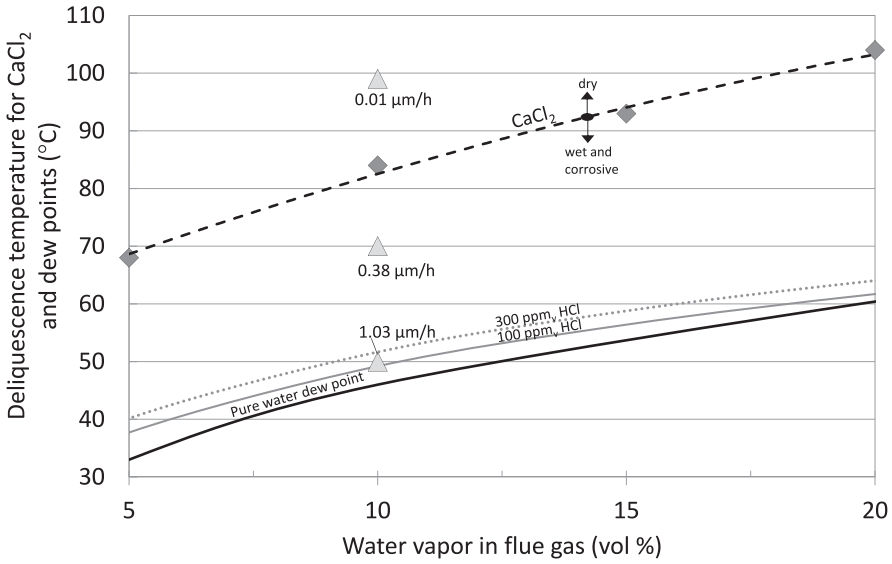

Fig. 13. Deliquescence temperature for $CaCl_2$, pure water, and HCl dew points as a function of water vapor concentration. Below the deliquescence curve, $CaCl_2$ will form an aqueous solution. The corrosion rates from the measurements at 50, 70, and 99 °C for Case 3 are also depicted. The $CaCl_2$ curve was calculated based on data from Vainio et al. [35] and HCl dew points by Kiang [31].

in the aqueous solution formed by deliquescence of $CaCl_2$ [35].

4. Summary and conclusions

Cold-end corrosion in a full-scale CFB boiler firing bituminous coal using different operational conditions was studied. Measurements of SO_3 and dew points were conducted before and after the ESP. A temperature-controlled corrosion probe was used to estimate the initial corrosion rate of carbon steel at various material temperatures. Deposits on the corrosion probe were collected and analyzed with SEM-EDX. Additionally, corrosion tests in a laboratory furnace were performed to understand the findings from the full-scale measurements.

Despite the relatively high sulfur content in the coal, the formation of SO_3 was very low (<0.1 ppm_v) and the risk for sulfuric acid related corrosion appears to be small – even with no limestone addition. No sulfuric acid dew point was detected with the dew point monitor. The relatively low furnace temperature in CFB combustion leads to low homogeneous conversion of SO_2 to SO_3. In addition, the high capturing potential of SO_3 by the alkali and alkaline earth metals in the fly ash contributes to the low SO_3. On the other hand, there seems to be a potential to corrosion caused by hygroscopic chloride salts under some conditions. Calcium chloride related corrosion may occur when limestone is used and the flue gases contain HCl. Most surprisingly, the risk of ammonium chloride related hygroscopic salt corrosion existed when operating the boiler at low loads.

The laboratory experiments confirmed that corrosion caused by water uptake by NH_4Cl is possible if the material temperature is too low. Additionally, dissociation of $NH_4Cl(s)$ at the steel surface may lead to a high local $NH_3(g)$ and HCl(g) concentration and subsequently corrosion. In a boiler, $NH_4Cl(s)$ in deposits may dissociate if the $NH_3(g)$, HCl(g), or temperature in the flue gas fluctuate.

CRediT authorship contribution statement

Emil Vainio: Investigation, Writing - original draft, Conceptualization, Visualization, Funding acquisition. **Kyösti Vänskä:** Investigation, Writing - review & editing. **Tor Laurén:** Resources, Writing - review & editing. **Patrik Yrjas:** Writing - review & editing, Conceptualization,

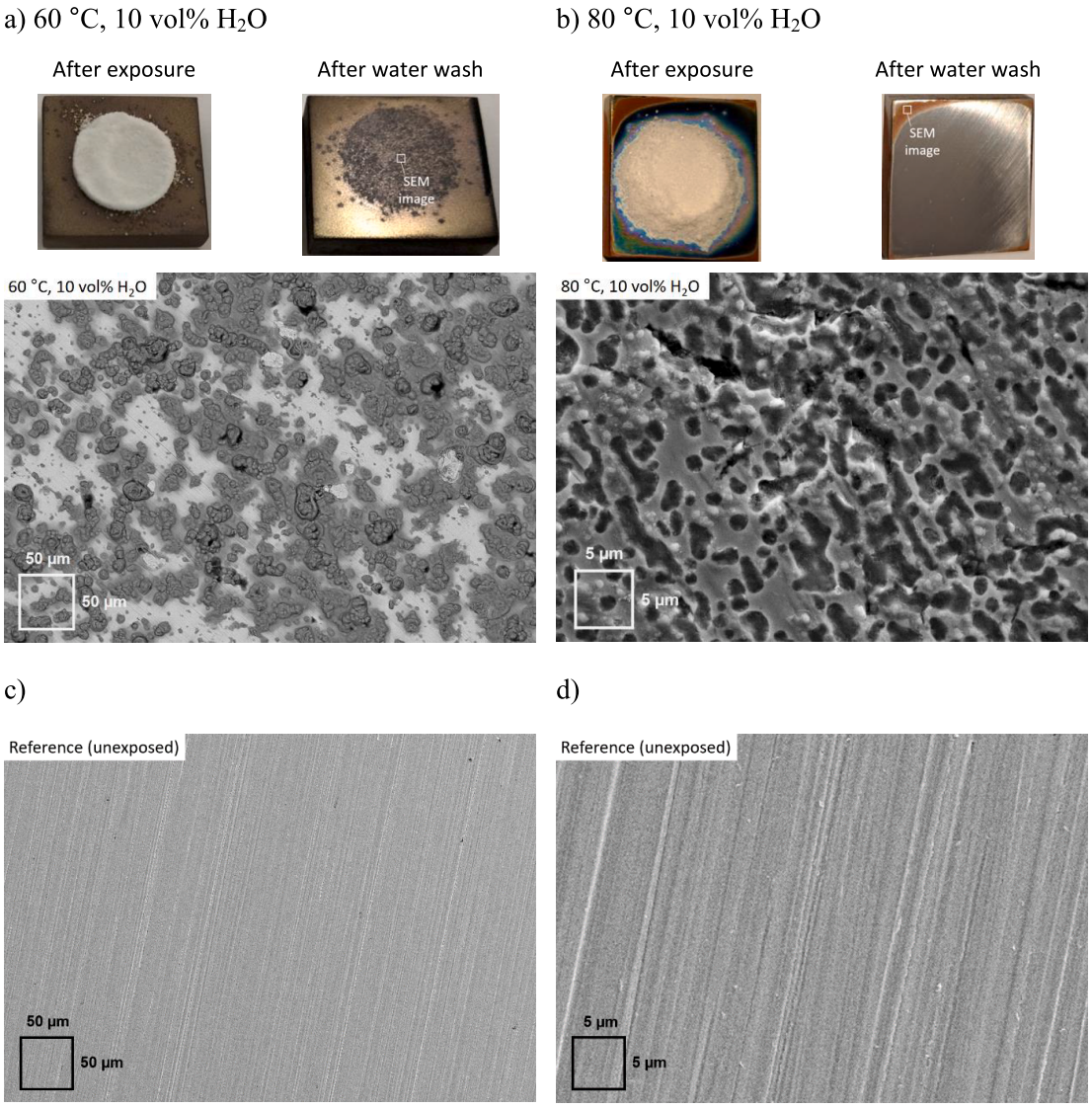

Fig. 14. SEM images and photographs of the P235GH coupons after exposure to NH_4Cl at 10 vol% H_2O at a) 60 °C and b) 80 °C. The locations of the images are indicated in the photographs. c) and d) are reference SEM images of the unexposed steel coupons.

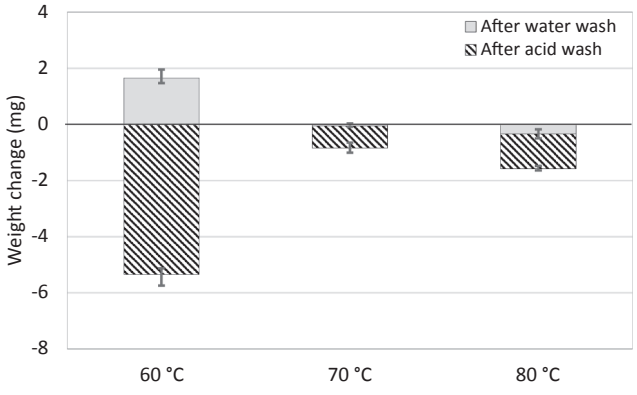

Fig. 15. Weight changes of P235GH after exposure to NH_4Cl at 10 vol% H_2O and 5 vol% O_2 for 4 h at various temperatures and after removing the corrosion products with water and citric acid.

Funding acquisition. **Edgardo Coda Zabetta:** Writing - review & editing, Conceptualization. **Mikko Hupa:** Writing - review & editing, Conceptualization, Funding acquisition. **Leena Hupa:** Writing - review & editing, Funding acquisition.

Declaration of Competing Interest

The authors declare that they have no known competing financial interests or personal relationships that could have appeared to influence the work reported in this paper.

Acknowledgments

This work has been carried out within the industrial consortium in Åbo Akademi University combustion research supported by the companies: Andritz Oy, Valmet Technologies Oy, Amec Foster Wheeler Energia Oy, UPM-Kymmene Oyj, Clyde Bergemann GmbH, International Paper Inc., and Top Analytica Oy Ab. Support from the National

Technology Agency of Finland (Tekes) and Academy of Finland (Decision No. 289869 and 333917) is gratefully acknowledged.

References

[1] Piper J, Van Vliet H. Effect of temperature variation on composition, fouling tendency, and corrosiveness of combustion gas from a pulverized-fuel-fired steam generator. Trans ASME 1958;80:1251–63.

[2] Mobin M, Malik AU, Al-Hajri M. J Fail Anal Prevent 2008;8(1):69–74.

[3] Spörl R, Walker J, Belo L, Shah K, Stanger R, Maier J, et al. SO_3 Emissions and Removal by Ash in Coal-Fired Oxy-Fuel Combustion. Energy Fuels 2014;28(8):5296–306.

[4] Vainio E, Kinnunen H, Laurén T, Brink A, Yrjas P, DeMartini N, et al. Low-temperature corrosion in co-combustion of biomass and solid recovered fuels. Fuel 2016;184:957–65.

[5] Tan YW, Croiset E, Douglas MA, Thambimuthu KV. Combustion characteristics of coal in a mixture of oxygen and recycled flue gas. Fuel 2006;85(4):507–12.

[6] Marier P, Dibbs HP. The catalytic conversion of SO_2 to SO_3 by fly ash and the capture of SO_2 and SO_3 by CaO and MgO. Thermochim Acta 1974;8(1–2):155–65.

[7] Glarborg P, Marshall P. Mechanism and modeling of the formation of gaseous alkali sulfates. Combust Flame 2005;141(1–2):22–39.

[8] Iisa K, Lu Y, Salmenoja K. Sulfation of Potassium Chloride at Combustion Conditions. Energy Fuels 1999;13(6):1184–90.

[9] Kassman H, Bäfver L, Åmand L-E. The importance of SO_2 and SO_3 for sulphation of gaseous KCl – An experimental investigation in a biomass fired CFB boiler. Combust Flame 2010;157(9):1649–57.

[10] Belo LP, Elliott LK, Stanger RJ, Sporl R, Shah KV, Maier J, et al. High-Temperature Conversion of SO_2 to SO_3: Homogeneous Experiments and Catalytic Effect of Fly Ash from Air and Oxy-fuel Firing. Energy Fuels 2014;28:7243–51.

[11] Fleig D, Alzueta MU, Normann F, Abián M, Andersson K, Johnsson F. Measurement and modeling of sulfur trioxide formation in a flow reactor under post-flame conditions. Combust Flame 2013;160:1142–51.

[12] Bennett RP. Chemical reduction of sulfur trioxide and particulates from heavy oils. Preprints of Papers - Am Chem Soc Div Fuel Chem 1976;21(1):35–42.

[13] Khan WZ, Gibbs BM, Ayaganova A. Emissions of SO_3 from a Coal-Fired Fluidized Bed under Normal and Staged Combustion. ISRN Environ Chem 2013. https://doi.org/10.1155/2013/514751.

[14] Bao J, Mao L, Zhang Y, Fang H, Shi Y, Yang L, et al. Effect of selective catalytic reduction system on fine particle emission characteristics. Energy Fuels 2016;30(2):1325–34.

[15] Menasha J, Dunn-Rankin D, Muzio L, Stallings J. Ammonium bisulfate formation temperature in a bench-scale single-channel air preheater. Fuel 2011;90(7):2445–53.

[16] Vainio E. Fate of fuel-bound nitrogen and sulfur in biomass-fired industrial boilers. Ph.D. thesis, Laboratory of Inorganic Chemistry, Åbo Akademi University 2014. <http://urn.fi/URN:ISBN:978-952-12-3010-3>.

[17] Verhoff FH, Banchero JT-J. Predicting Dew Points of Gases. Chem. Eng. Prog. 1974;70(8):71–2.

[18] Lindau L, Goldschmidt B. Low temperature corrosion in bark fueled small boilers. 2008 Värmeforsk Services AB, report M9-835.

[19] Müller H, Brell S, Schneider M. Corrosion Caused by Dew Point and Deliquescent Salts in the Boiler and Flue Gas Cleaning. Waste Manage 2012;4:343–58.

[20] Vainio E, DeMartini N, Hupa M, Hupa L. Role of ash-forming elements on low-temperature corrosion in biomass boilers, Impacts of fuel quality on power production, the 26th international conference, September 19-23, 2016b, Prague, Czech Republic.

[21] Retschitzegger S, Brunner T, Obernberger I. Low-Temperature Corrosion in Biomass Boilers Fired with Chemically Untreated Wood Chips and Bark. Energy Fuels 2015;29(6):3913–21.

[22] Brunner T, Reisenhofer E, Obernberger I, Kanzian W, Forstinger M, Vallant R. Low-Temperature Corrosion in Biomass-Fired Combustion Plants - Online Measurement of Corrosion Rates, Acid Dew Points and Deliquescence Corrosion. 25th European Biomass Conference and Exhibition, 12-15 June 2017, Stockholm, Sweden.

[23] Pan P, Zhou W, Chen H, Zhang N. Investigation on the Corrosion of the Elbows in the Flue Gas Cooler of a 600 MW Coal-Fired Power Plant. ACS Omega 2020;5:32551–63.

[24] Herzog T, Müller W, Spiegel W, Brell J, Molitor D, Schneider D. In: Corrosion caused by dewpoint and deliquescent salts in the boiler and flue gas cleaning. VGL: KG Thome-Kozmiensky og M. Neuruppin: TK Verlag; 2012. p. 429–60.

[25] Cullis C, Mulcahy M. The kinetics of combustion of gaseous sulphur compounds. Combust Flame 1972;18:225–92.

[26] Sheng C, Xu M, Zhang J, Xu Y. Comparison of sulphur retention by coal ash in different types of combustors. Fuel Process Technol 2000;64:1–11.

[27] Zhang J, Han C-L, Yan Z, Liu K, Xu Y, Sheng C-D, et al. The Varying Characterization of Alkali Metals (Na, K) from Coal during the Initial Stage of Coal Combustion. Energy Fuels 2001;15(4):786–93.

[28] Ferrer E, Aho M, Silvennoinen J, Nurminen R-V. Fluidized bed combustion of refuse-derived fuel in presence of protective coal ash. Fuel Process Technol 2005;87:33–44.

[29] Vainio E, Fleig D, Brink A, Andersson K, Johnsson F, Hupa M. Experimental Evaluation and Field Application of a Salt Method for SO_3 Measurement in Flue Gases. Energy Fuels 2013;27(5):2767–75.

[30] Laurén T. Methods and instruments for characterizing deposit buildup on heat exchangers in combustion plants. Licentiate thesis. Laboratory of Inorganic Chemistry, Åbo Akademi University; 2007.

[31] Kiang YH. Predicting dew points of acid gasses. Chem Eng 1981;9:127–8.

[32] Glarborg P, Marshall P. Mechanism and modeling of the formation of gaseous alkali sulfates. Combust Flame 2005;41(1–2):22–39.

[33] Åmand L-E, Leckner B, Andersson S. Formation of N_2O in Circulating Fluidized Bed Boilers. Energy Fuels 1991;5:815–23.

[34] Bale CW, Belisle E, Chartrand P, Decterov SA, Eriksson G, Gheribi AE, Hack K, Jung I-H, Kang Y-B, Melancon J, Pelton AD, Petersen S, Robelin C, Sangster J, Spencer P, Van Ende M-A. In: CALPHAD: Comput. Coupling Phase Diagrams Thermochem.; 2016. p. 35–53.

[35] Vainio E, DeMartini N, Hupa L, Amand L-E, Richards T, Hupa M. Hygroscopic Properties of Calcium Chloride and its Role on Cold-End Corrosion in Biomass Combustion. Energy Fuels 2019;13:11913–22.

[36] Millero FJ, Huang F. Solubility of Oxygen in Aqueous Solutions of KCl, K_2SO_4, and $CaCl_2$ as a Function of Concentration and Temperature. J Chem Eng Data 2003;48:1050–4.

[37] Borgmann CW. Initial Corrosion Rate of Mild Steel Influence of the cation. Ind Eng Chem 1937;29(7):814–21.

[38] Adams JR, Merz AR. Hygroscopicity of fertilizer materials and mixtures, lndust. Enff. Chem. 1929;21:305–10.

[39] Zhu RS, Wang JH, Lin MC. Sublimation of Ammonium Salts: A Mechanism Revealed by a First-Principles Study of the NH_4Cl System. J Phys Chem C 2007;111:13831–8.